Calcif Tissue Int (2004) 74:437–447
DOI: 10.1007/s00223-003-0071-z

Calcified Tissue International


# Comparison of Microcomputed Tomographic and Microradiographic Measurements of Cortical Bone Porosity

**D. M. L. Cooper,[1] J. R. Matyas,[2] M. A. Katzenberg,[3] B. Hallgrimsson[4]**

[1]Departments of Archaeology and Medical Science, and the Joint Injury and Arthritis Research Group, University of Calgary, T2N 4N1, Calgary, Alberta, Canada
[2]Departments of Cell Biology & Anatomy and Pathology & Laboratory Medicine, and the Joint Injury and Arthritis Research Group, University of Calgary, T2N 4N1, Calgary, Alberta, Canada
[3]Department of Archaeology, University of Calgary, T2N 4N1, Calgary, Alberta, Canada
[4]Department of Cell Biology & Anatomy, and the Joint Injury and Arthritis Research Group, University of Calgary, 3330 Hospital Drive NW, T2N 4N1, Calgary, Alberta, Canada

Received: 27 March 2003 / Accepted: 30 September 2003 / Online publication: 17 February 2004

**Abstract.** Cortical bone is perforated by a network of canals that have a significant impact upon its material properties. Microcomputed tomography offers the possibility of noninvasively visualizing and quantifying cortical pores in both two and three dimensions. Establishing how two-dimensional (2D) microcomputed tomographic (μCT) analysis compares with conventional methods for analyzing cortical porosity is an important prerequisite for the wider adoption of this technique and the development of three-dimensional (3D) analysis. Therefore, we compared porosity-related parameters from 2D microcomputed tomographic images with those from matching microradiographic sections. Samples from five human femora were scanned at a 10-μm resolution and then sequentially sectioned and microradiographed. An average of eight image pairs were produced from each femur (total, $n = 41$). The repeatability and comparability of the two techniques was assessed for three parameters; cortical porosity (%), mean pore area ($\mu m^2$), and pore density (pores/$mm^2$). For repeatability, no significant difference ($P > 0.05$) was found between the two methods for cortical porosity and mean pore area; however, pore density differed significantly ($P < 0.001$). For comparability, the bias (± error) between the methods was found to be 0.51% (±0.31%) for cortical porosity and −155 $\mu m^2$ (±293 $\mu m^2$) for mean pore area. The bias for pore density was dependent upon measurement size with microcomputed tomographic images having 14% (±9.3%) fewer pores per millimeter squared. The qualitative and quantitative similarities between the two techniques demonstrated the utility of 2D microcomputed tomographic for cortical porosity analysis. However, the relatively poor results for pore density revealed that a higher resolution (< 10 μm) is needed to consistently visualize all cortical pores in human bone.

**Key words:** Cortical porosity — Bone histology and histomorphometry — Microcomputed tomography — Microradiography — Bone microstructure

*Correspondence to:* B. Hallgrimsson; E-mail: bhallgri@ucalgary.ca

Cortical bone is perforated by a network of canals that contain loose connective tissue and provide conduits for the passage of neurovascular structures [1]. The creation of these canals is an intrinsic aspect of the processes of modeling and remodeling that form and rework bone. Bone formed by modeling incorporates primary porous spaces that develop into primary osteons. Remodeling creates Haversian systems (secondary osteons) through the initial destruction of cylindrical packets of bone followed by circumferential deposition of new bony lamellae within these resorption spaces. Haversian systems, which occupy the majority of adult human compact bone, have a complex, branched arrangement [2, 3] and, as a consequence, so do their central (haversian) canals. The general orientation of haversian systems varies within and among bones, and it is believed that this variation reflects the prevailing mechanical environment [4, 5]. When viewed in cross-section, the network of cortical canals appears as a collection of distinct pores. The relative area occupied by these pores, cortical porosity, is an important parameter affecting the mechanical properties of cortical bone [6–9]. Further, it has been demonstrated that the cross-sectional spatial arrangement and dimensions of cortical pores influence the risk of fracture [10–14]. Yet, the full functional significance of the cortical pore network remains poorly understood. A better understanding of the three-dimensional (3D) arrangement of cortical canals will not only improve the interpretation of bone's material properties but will also elucidate the processes by which cortical bone forms and adapts.

To date, the analysis of porosity in cortical bone has been largely limited to the evaluation of two-dimensional (2D) sections. Reconstruction based upon serial histological sectioning does provide a means of examining cortical canals in three dimensions [2, 15], but this technique is both tedious and destructive. The devel-

opment of alternative methods has been impeded by the small scale of the canals, which is beyond the resolution of conventional nondestructive imaging techniques. The average diameters of porous structures in human bone range from approximately 30 μm for haversian canals, up to 400 μm for resorptive cutting cones [16, 17]. The spatial resolution of microcomputed tomographic (μCT) scanners continues to improve and, although resolutions below 2 μm are possible by using a synchrotron radiation source [18], commercially available desktop μCT scanners are capable of scan resolutions as low as 5 μm. Therefore, microcomputed tomography is the first imaging technology capable of resolving cortical pores in human bone [17] and visualizing them in three dimensions [19]. As such, this technology promises to provide an efficient, nondestructive, means of 3D quantitative analysis of cortical porosity in a manner analogous to its growing application for trabecular bone analysis [20]. However, as has been done in numerous studies of trabecular bone [21–29], it is necessary to establish how μCT-based measurements compare with those from conventional histological methods. Therefore, the goal of this study was to examine how comparable 2D μCT measurements of porosity-related parameters are to those from corresponding microradiographs of ground sections.

## Materials and Methods

Cortical bone samples were obtained from five, disarticulated and previously defleshed adult human femora of unknown age and sex from the anatomical teaching collection at the University of Calgary Faculty of Medicine. The bones showed no gross sign of fracture or pathological lesions. Rectangular blocks measuring approximately 5 by 12 mm (Fig. 1) were removed from the anterior midshaft of each femur using a handheld rotary saw (Dremel, Racine, WI, USA). The long axes of the samples were aligned with the long axes of the femora.

### *Microcomputed Tomographic Imaging*

All imaging was performed at the University of Calgary 3D Morphometrics Laboratory. The samples were scanned using a SkyScan 1072 (Aartselaar, Belgium) x-ray microtomograph at 27-times magnification. The samples were rotated through 180 degrees at a rotation step of 0.45 degrees. The x-ray settings were standardized to 100 kV and 100 μA, with an exposure time of 5.9 seconds per frame. Four-frame averaging was used to improve the signal-to-noise ratio. A 1 mm-thick aluminum filter and a beam-hardening correction algorithm were employed to minimize beam-hardening artifacts (SkyScan hardware/software). The scan time for each sample was approximately 4 hours. A cone beam algorithm was used to reconstruct 8-bit cross-sectional images (1024 × 1024 pixels), with each pixel representing a 10 $\mu m^3$ voxel. Each scan yielded 900 contiguous slices, spanning 9 mm along the length of the sample. The 10-μm resolution was chosen because it allowed the entire cortical thickness of the samples, which averaged approximately 5 mm, to be included within the reconstructed field of view. To further reduce image noise and preserve detail in three dimensions, the image series were passed through a 3D median filter with a 3 × 3 × 3 cubic kernel by using Analyze 4.0 (Analyze Direct, Lenexa, KS).

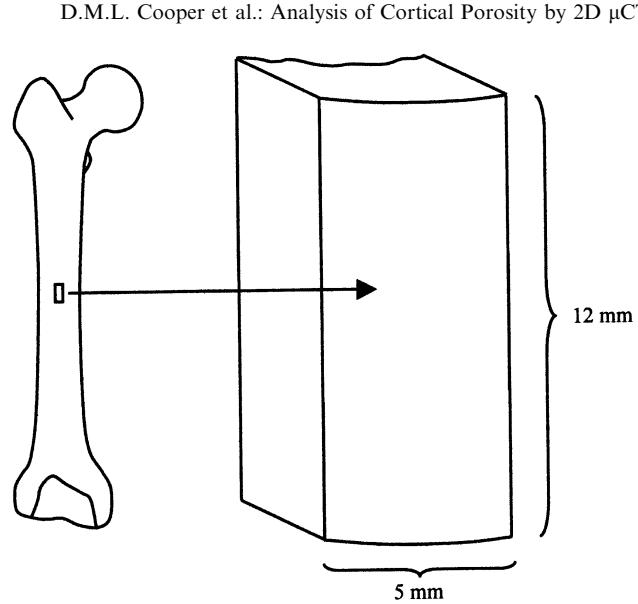


**Fig. 1.** Sample size and location.

### *Microradiography*

After μCT scanning, sequential ground sections were prepared from the bone samples in the same plane from which the cross-sectional images were acquired. Sequential 250-μm-thick sections were cut with an Isomet diamond wafer saw (Buehler, Lake Bluff, IL) at a spacing of approximately 600 μm (due to the kerf). This produced 10 sections from within the same volume that was previously scanned for each sample. The sections were lapped by hand to 100 μm with constant irrigation using distilled water. After lapping, the sections were cleaned by ultrasonification in distilled water for 10 minutes. Contact microradiographs of the ground sections were prepared by using a Faxitron (Hewlett-Packard, McMinnville, OR) radiation source. Type 3 Orthofilm (Kodak, Rochester, NY) was exposed at 25 kV for 15 minutes at a distance of 20 cm from the source. The developed films were illuminated with transmitted light and digitized with a Spot Insight camera (Diagnostic Instruments, Sterling Heights, MI) mounted on an SZX12 microscope (Olympus, Melville, NY). Images were captured as 1200 × 1600-pixel matrices with a pixel resolution of 4.95 × 4.95 μm, roughly double that of the μCT images.

### *Image Processing*

Following the convention of Kuhn et al. [26] the 2D μCT images will be referred to as *slices* and the microradiographs as *sections*. Prior to analysis, it was necessary to modify a subset of the serial μCT slices to produce a single composite slice that was comparable to each of the corresponding microradiographic sections. This involved two processes: (1) matching the slice thickness to section thickness, and (2) matching the scale and orientation of the slices to that of the sections. The microradiographic sections represented the x-ray attenuation through the 100-μm thickness of the ground sections, whereas each μCT image represented a thinner 10-μm-thick slice. Therefore, for each section, the closest matching slice was found within the 900-slice data set for the corresponding sample. This matching slice was then averaged with its nine nearest neighbors (four down and five up), effectively producing a 100-μm-thick composite μCT slice (similar to Kuhn et al. [26]). The composite microcomputed tomographic slices and microradiographic sections were segmented using a local

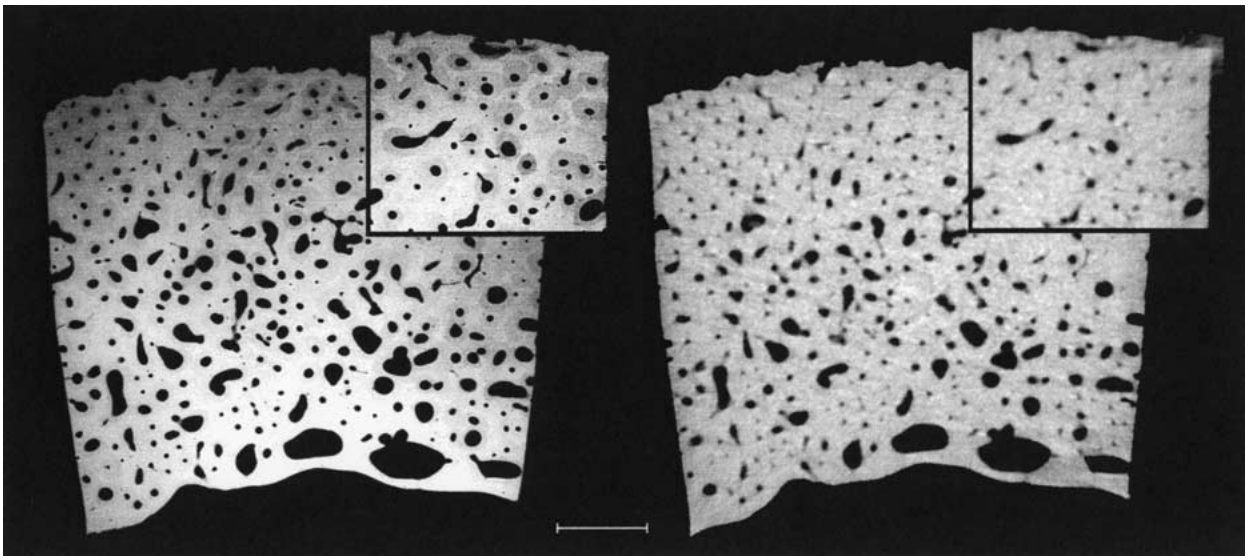

**Fig. 2.** Example of matching cross-sectional image sets (Femur 5, Section 2). Microradiograph (section) is on the left, composite μCT slice is on the right. Inset at upper right is magnified (1.3×) to demonstrate differences in density visible in the microradiograph (bar = 1 mm).

**Table 1.** Summary of results including mean (±SD) values for the two techniques and the differences (section-slice) between them by sample

| Sample (Femur) | 1 | 2 | 3 | 4 | 5 |
|---|---|---|---|---|---|
| Replicates (n) | 7 | 7 | 8 | 9 | 10 |
| Cortical porosity (%) | | | | | |
| Microradiograph | 7.43 (±0.61) | 5.29 (±0.42) | 4.57 (±0.28) | 3.44 (±0.33) | 12.21 (±1.03) |
| μCT | 6.53 (±0.28) | 4.55 (±0.27) | 4.17 (±0.40) | 3.09 (±0.28) | 12.07 (±0.81) |
| Difference | 0.90 | 0.74 | 0.40 | 0.35 | 0.14 |
| Mean Pore Area ($\mu m^2$) | | | | | |
| Microradiograph | 5366 (±588) | 4169 (±322) | 2790 (±148) | 3239 (±190) | 11,859 (±862) |
| μCT | 5663 (±747) | 3843 (±120) | 3182 (±214) | 3318 (±250) | 12,189 (±516) |
| Difference | −298 | 326 | −392 | −79 | −331 |
| Pore density (pores/$mm^2$) | | | | | |
| Microradiograph | 12.7 (±0.6) | 12.2 (±0.3) | 15.7 (±0.4) | 10.0 (±0.4) | 9.8 (±0.4) |
| μCT | 10.5 (±1.1) | 11.2 (±0.8) | 12.4 (±0.6) | 9.3 (±0.6) | 9.3 (±0.4) |
| Difference | 2.2 | 0.9 | 3.3 | 0.7 | 0.5 |

threshold algorithm (3D-Calculator V0.9, available at http://www.eur.nl/fgg/orthopaedics/Downloads.html) that utilizes a 3 × 3 Sobel edge-detection to determine gradients in the image grayscale values that represent object edges. These gradients then serve as the basis for determining localized threshold values that the software uses to divide the image into black and white representing pores and bone. Following segmentation, the composite μCT slices were scaled and rotated to match the size and orientation of their corresponding microradiographic section. All image processing and subsequent analysis was performed using ImageJ 1.27z (http://rsb.info.nih.gov/ij/).

### *Statistical Methods*

Comparisons between the microradiographic sections and the composite μCT slices were based on cortical porosity (%), mean pore area ($\mu m^2$), and pore density (pores/$mm^2$). Matching rectangular regions of interest were cropped from the midcortical field of the slices and sections. These regions were chosen such that trabecularization of the endosteal surface was avoided. The size of the regions was standardized for the slice and section pairs acquired from each of the five femoral samples, but varied somewhat between femora due to differences in the cortical thickness. Cortical porosity was measured from the binary images as the percentage of void pixels in the region of interest. All void pixels including those from osteonal canals (primary and haversian), Volkmann canals, and resorption spaces were included. The particle analysis function within ImageJ was used to count the number of individual pores and measure their areas. Pores bordering the image edges were included in pore number count but not in the calculation of mean pore area. This systematically overestimated pore number, but was not a concern in this comparative study. Pore density was calculated by dividing the number of pores by the area ($mm^2$) of the region of interest.

Statistical analysis was performed using SPSS 11.0.1 (SPSS Inc., Chicago, IL). The results from the two methods were compared in accordance with the approach outlined by Altman and Bland [30]. Their method distinguishes between the analysis of repeatability and comparability. Repeatability is measured as the "within-subject standard deviation of the

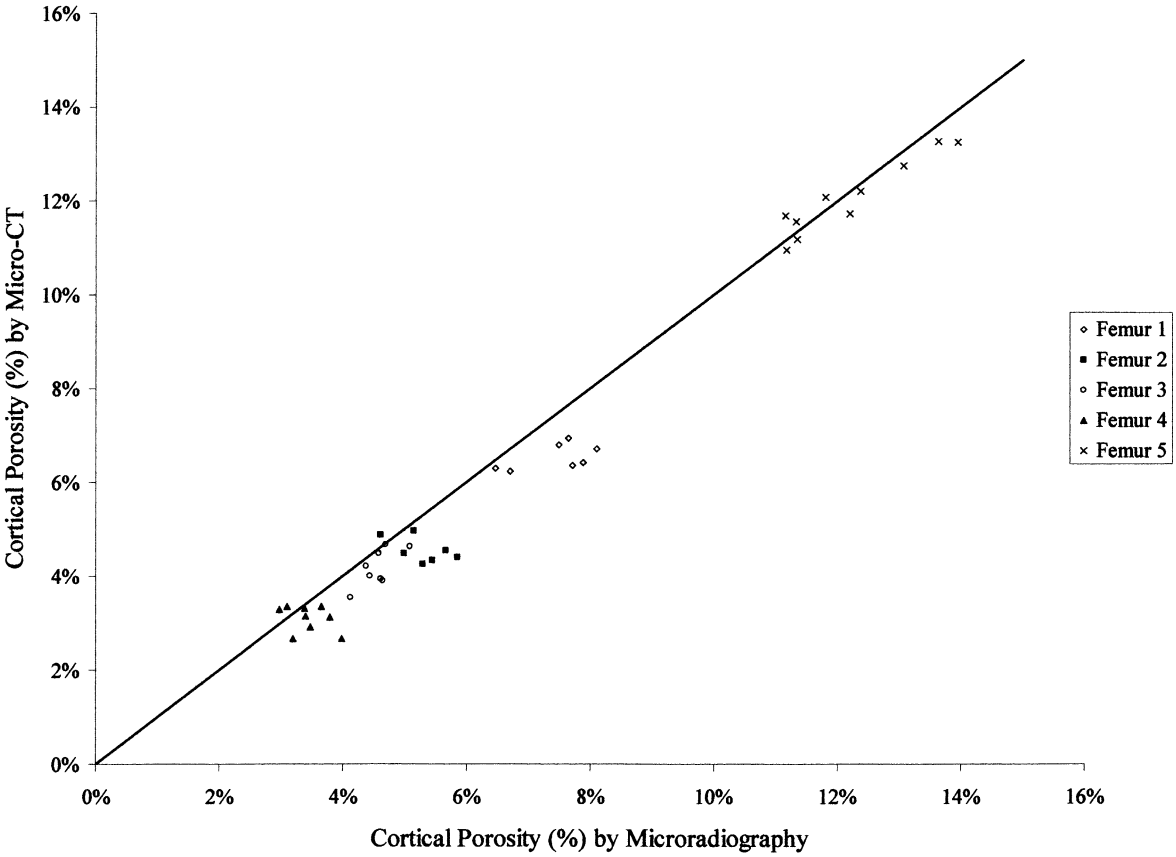


**Fig. 3.** Scatterplot for cortical porosity measured by microradiography versus μCT (micro-CT) ($n$ = 41). Line of identity is shown.

replicates'' [30]. In our analysis, the slices and sections from each femoral sample were treated as repeated measures or replicates of a single individual. Provided that repeatability is independent of the magnitude of the measurements, the standard deviation of the residuals (replicates-sample mean) provides a pooled measure of repeatability across samples. For the current study, the repeatability of each method (microradiography and μCT) was assessed separately for each of the three parameters (cortical porosity, mean pore area, and pore density). Differences in the repeatability of the two methods for each of the parameters were assessed with F tests.

Comparability examines the extent to which to one method agrees with another, addressing the question of whether they, on average, measure the same thing [30]. This is assessed through an analysis of the differences between the two techniques. Bias is measured by the mean of the differences between the techniques, while random error about the bias is measured by the standard deviation of these differences [30]. This approach was favored because both techniques ( μCT and microradiography) are considered to acquire measurements with error, and a single measure of bias and relative error are produced. This is in contrast to least squares regression, which provides a means of establishing how well one method predicts another, and is essentially a calibration approach. Further, in least squares regression, error depends upon distance from the mean, and thus is more difficult to interpret. In our study, the analysis of comparability was conducted on the means of the replicates from each sample. Although bias is unaffected by the use of mean values, error is underestimated [30]. Therefore, to gain a better picture of the sources of variation in our design and their significance we followed the recommendation of Altman and Bland in applying an analysis of variance adopted to our data structure [30]. We performed a fully factorial nested analysis of variance (ANOVA), with method and sample as main effects, and the corresponding slice–section pairs nested within samples.

In the Altman and Bland [30] approach, both analysis of repeatability and comparability require that the standard deviation is independent of the magnitude of the measurement. Because the method depends on the analysis of residuals, if the standard deviation is not independent of the mean, bias becomes a function of the mean. When the standard deviation is correlated with the mean, Altman and Bland recommend applying a log transformation to the data.

## Results

The composite μCT slices and the microradiographic sections were strikingly similar, and both the overall geometry and location of the pores within the cortex matched (Fig. 2). The higher spatial resolution of the sections resulted in better visualization of smaller pores than in the slices. Secondary osteons of varying densities were discernable in the sections, but no clear variations in mineral density were observed in the slices. In addition, features such as cementing lines and lamellae were not discernable in the slices, and, therefore, it was not possible to differentiate between primary and secondary osteons.

A total of 41 matching slice–section pairs were analyzed from the five femora. Nine of the potential 50 image pairs were excluded because of damage during

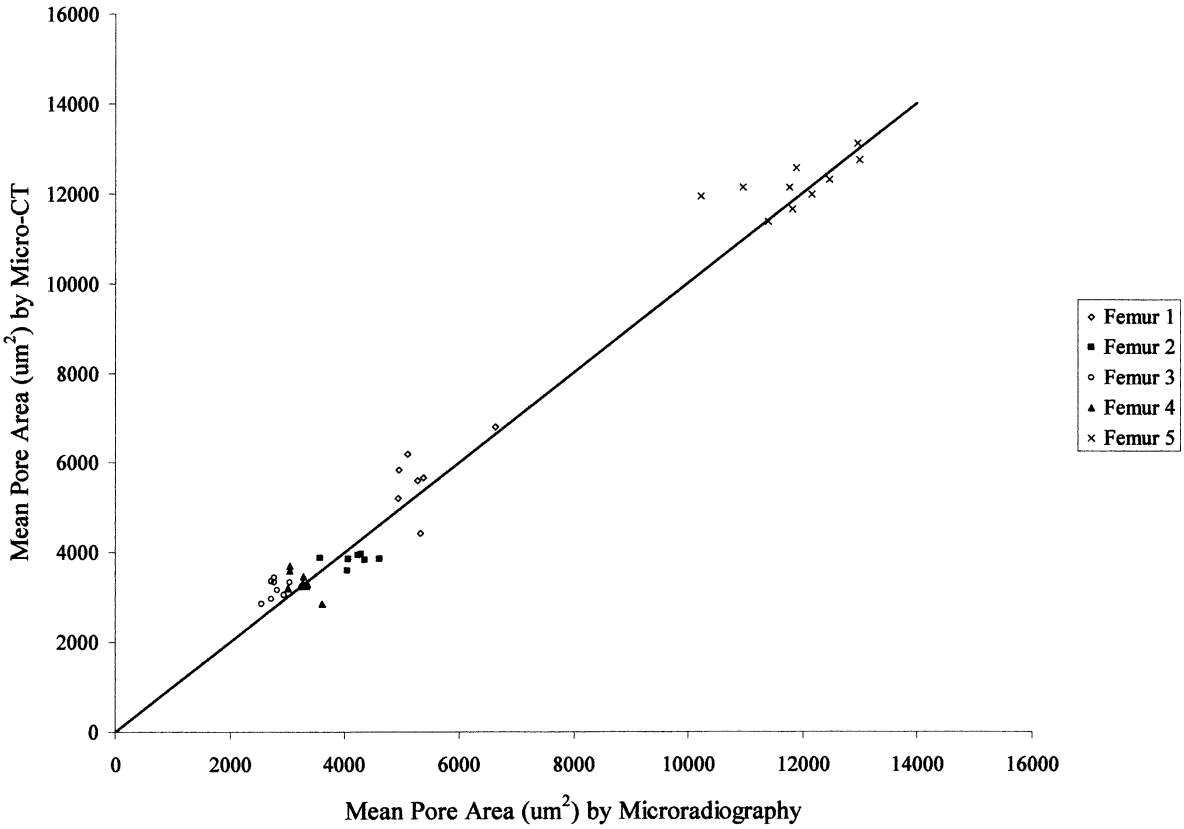


**Fig. 4.** Scatterplot for mean pore area measured by microradiography versus μCT (micro-CT) ($n = 41$). Line of identity is shown.

sectioning or artifacts in the image data. The region of interest that was analyzed ranged from 14.7 to 21.6 mm$^2$ (mean, 18.5 mm$^2$). The mean values, standard deviations, and differences between techniques for the three parameters are listed by sample in Table 1. Bivariate plots of the raw results for cortical porosity, mean pore area, and pore density are presented in Figures 3–5, respectively. The scatter of points for cortical porosity and mean pore area fall close to the line of identity. The plot for pore density demonstrates a deviation away from identity, with slice measurements becoming increasingly lower than those from the corresponding sections. Bland-Altman plots for cortical porosity, mean pore area, and pore density are presented in Figures 6–8, respectively.

For the analysis of repeatability, cortical porosity measured by both methods, and mean pore area measured by microradiography, yielded significant ($P < 0.05$) correlation coefficients between the standard deviation and mean value of the replicates. Therefore, a log transformation was used on the raw data for all three parameters. After back-transformation of the log values, the repeatability (standard deviation of the residuals) reflects a percentage of the measurement magnitude rather than an absolute value [30]. A lower percentage reflects a more consistent result between replicates. Repeatability of the sections was 7.8%, 6.9%, and 3.4% for cortical porosity, mean pore size, and pore density, respectively. Repeatability of the slices was 7.3%, 7.5%, and 6.2% for cortical porosity, mean pore size, and pore density, respectively. These values should be interpreted as overestimates, as they confound real biological variation within each block and actual repeatability of the measurement. F tests revealed no significant differences in repeatability ($P < 0.05$) between the two methods for cortical porosity and mean pore area; however, pore density differed significantly ($P < 0.001$).

In the analysis of comparability, no significant ($P > 0.05$) linear relationship was found between the magnitude of the differences and the mean measurements for either cortical porosity or mean pore area. The bias (±error) between the sections and slices was found to be 0.51% (±0.31%) for cortical porosity and −155 μm$^2$ (±293 μm$^2$) for mean pore area. Log transformation was used on the pore density data to remove the significant ($P < 0.05$) linear relationship. Bias (±error) between the sections and slices for this parameter, was found to be 14% (±9.3%) of the magnitude of the measurement. Table 2 summarizes the results of the ANOVA. For all three parameters, the femoral samples themselves were the largest (mean square) significant source of variation ($P < 0.001$), reflecting the presence of real biological variation among the samples. The

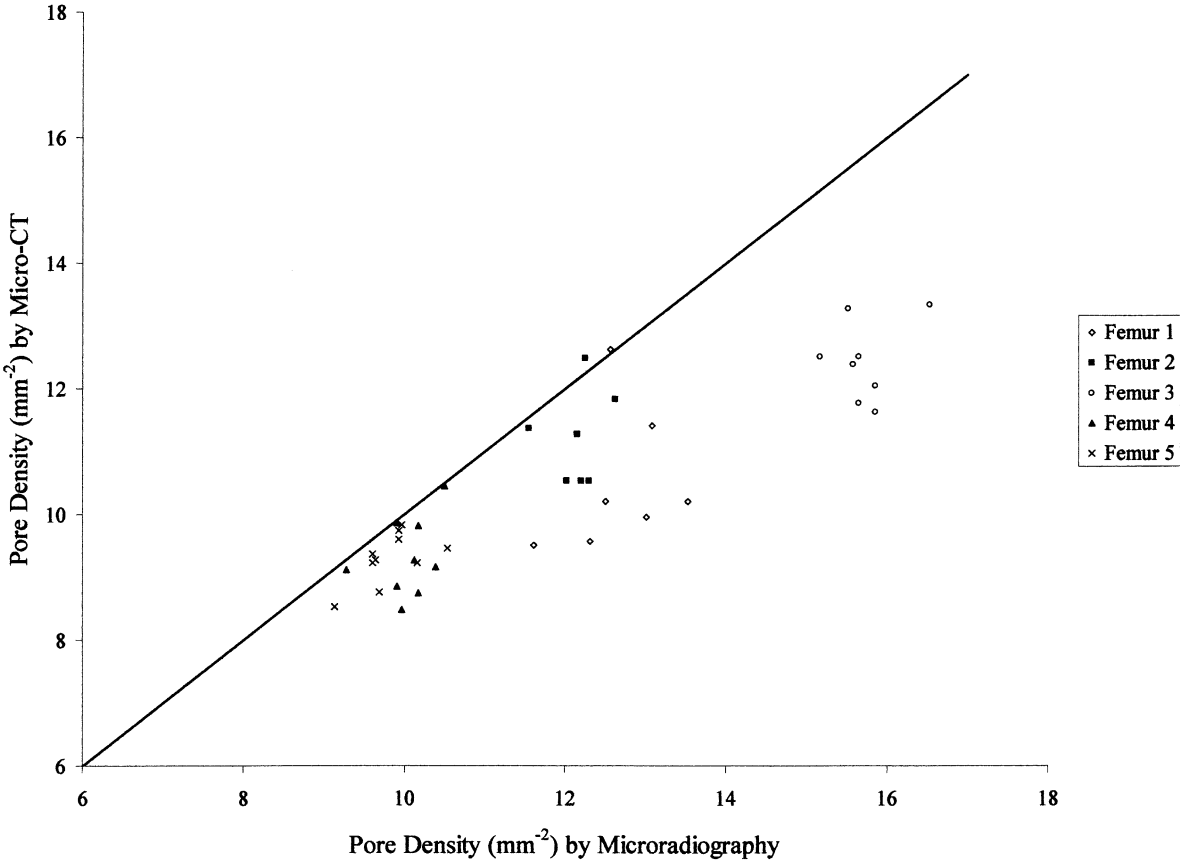


**Fig. 5.** Scatterplot for pore density measured by microradiography versus μCT (micro-CT) ($n = 41$). Line of identity is shown.

difference between the means obtained from the two methods was significant ($P < 0.001$) for cortical porosity and pore density, and almost so ($P = 0.054$) for mean pore area. The method by sample interaction for cortical porosity ($P = 0.014$) and pore density ($P < 0.05$) were significant, whereas that for mean pore area nearly so ($P = 0.050$). Slice–section pairs nested within samples were a significant ($P \leq 0.001$) source of variation for cortical porosity and mean pore area, and nearly so for pore density ($P = 0.051$). This factor reflects both measurement error and real biological variation within each block.

## Discussion

Cortical porosity plays a significant role in determining the material properties of normal and diseased bone and is, therefore, of considerable interest to a number of areas of research. The commercial availability of high-resolution μCT systems makes this technology a potentially attractive and efficient tool for the nondestructive evaluation of cortical bone porosity. Therefore, the proximate goal of this study was to assess whether 2D μCT produces measurements in human bone comparable to those of conventional microradiographs. However, because 3D μCT is based upon serial reconstruction of 2D slices, validation of 2D μCT also serves a necessary step towards the ultimate development of 3D analysis of cortical bone porosity. Based upon the results of the ANOVA, the differences between the μCT and microradiographic values were significant, or nearly so in the case of mean pore area, for all three parameters. However, despite these differences, for two of the three parameters (cortical porosity and mean pore area) repeatability was equivalent for the two techniques and the biases between them were relatively small. The bias for cortical porosity was about one half a percent (0.51%), indicating that the μCT slices were just slightly underestimating porosity relative to the corresponding sections. The bias for mean pore area was $-155$ μm$^2$ and, considering that each pixel in the μCT slices was 100 μm$^2$ ($10 \times 10$ μm), this bias equates to an average overestimation of $< 2$ pixels per pore in the μCT slices versus the sections. Based upon these findings, we believe that 2D μCT is an effective technique for the nondestructive assessment of cortical porosity in human bone.

The differences between the microradiographic and μCT measurements were influenced by many factors, including errors associated with image acquisition and processing, resolution, and specimen preparation. A key factor was imperfect image alignment. The alignment of

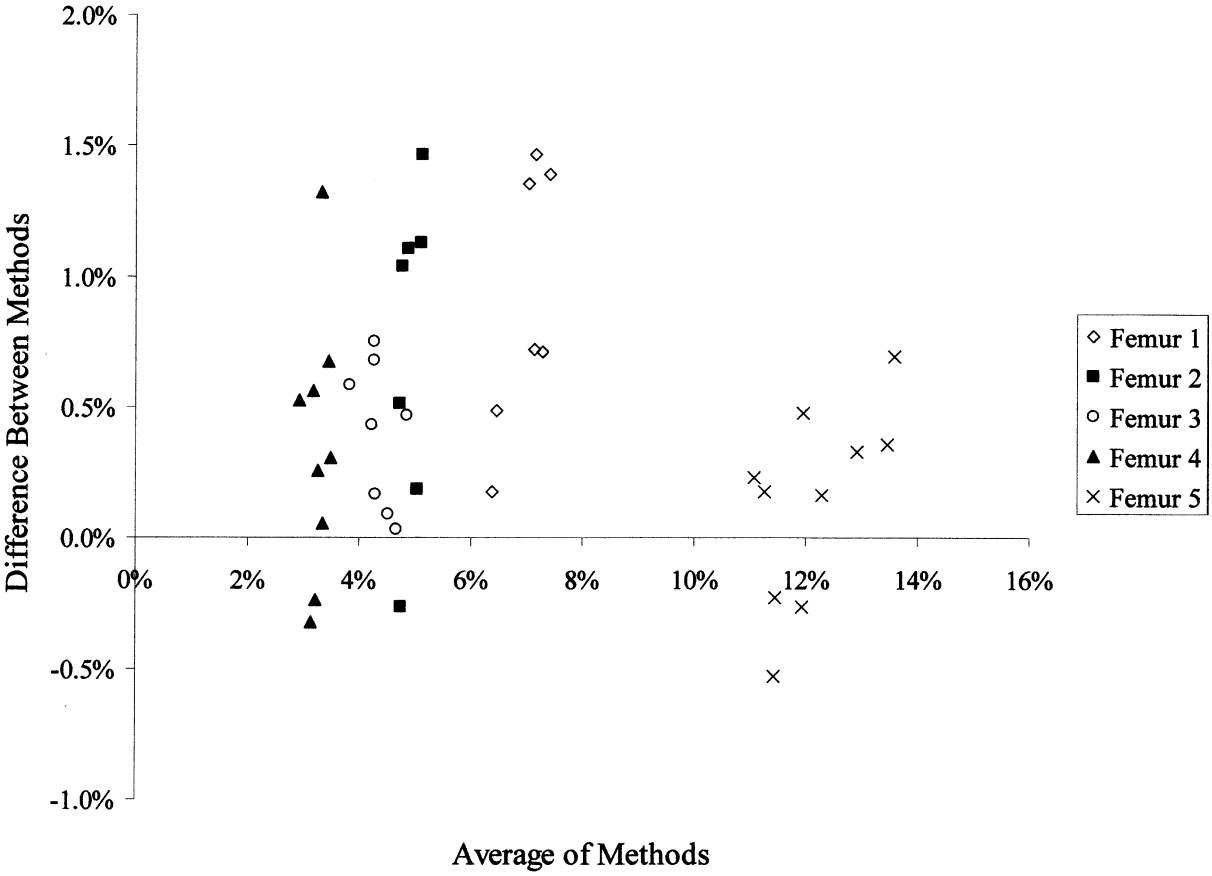


**Fig. 6.** Bland-Altman plot of the differences between methods for cortical porosity (%).

the bone sample in the μCT scanner and in the diamond wafer saw was done manually, and, therefore, a perfect match was impossible. Hence, the composite μCT slices sampled slightly different volumes than the matching ground sections did, and some differences in the measured parameters were expected. Nonetheless, the visual match between the image pairs was excellent, providing a sound basis for assessing the quantitative differences between the two methods.

Image segmentation was another primary concern, as thresholds significantly influence morphological measurements. Several validation studies of trabecular bone morphometry have addressed this issue, some presenting data from multiple thresholds [23–25]. Two approaches, global and local thresholding, have been employed to segment grayscale images into binary black-and-white images to facilitate automated morphological analysis. With global thresholding, a single grayscale value is assigned as a threshold above which pixels are converted to black and below which pixels are converted to white (or vice versa). Global thresholding can be problematic when applied to μCT image data because of the variation in x-ray attenuation associated with differences in geometry and density, both within and between samples [26, 31]. In contrast, local thresholding is based upon local grayscale fluctuations within an image, and can account for changes in x-ray attenuation, thereby providing a more accurate definition of object edges. Therefore, to optimize the inclusion of small pores and compensate for grayscale fluctuations, such as those caused by beam-hardening, we chose to use a local threshold algorithm. Moreover, the same algorithm was applied to the slices and the sections, which ensured that the comparisons of porosity-related parameters were based upon differences between the images rather than on the method of segmentation or software used. The excellent agreement between the repeatability of the microradiographic and μCT measurements for cortical porosity and mean pore area indicated that segmentation was effective and consistent. The relatively poor repeatability for μCT-based pore density, was more likely due to the limitation of the 10-μm scan resolution than the segmentation algorithm.

The visualization of smaller pores was relatively poorer in the slices as compared with the sections. This was primarily a consequence of the partial volume effect. In essence, each voxel in a tomograph represents the average x-ray attenuation at its corresponding volume within the target sample. If that volume contains more than one object (in our case, air and bone) its grayscale value represents the average attenuation of these objects. As target objects become smaller, approaching the

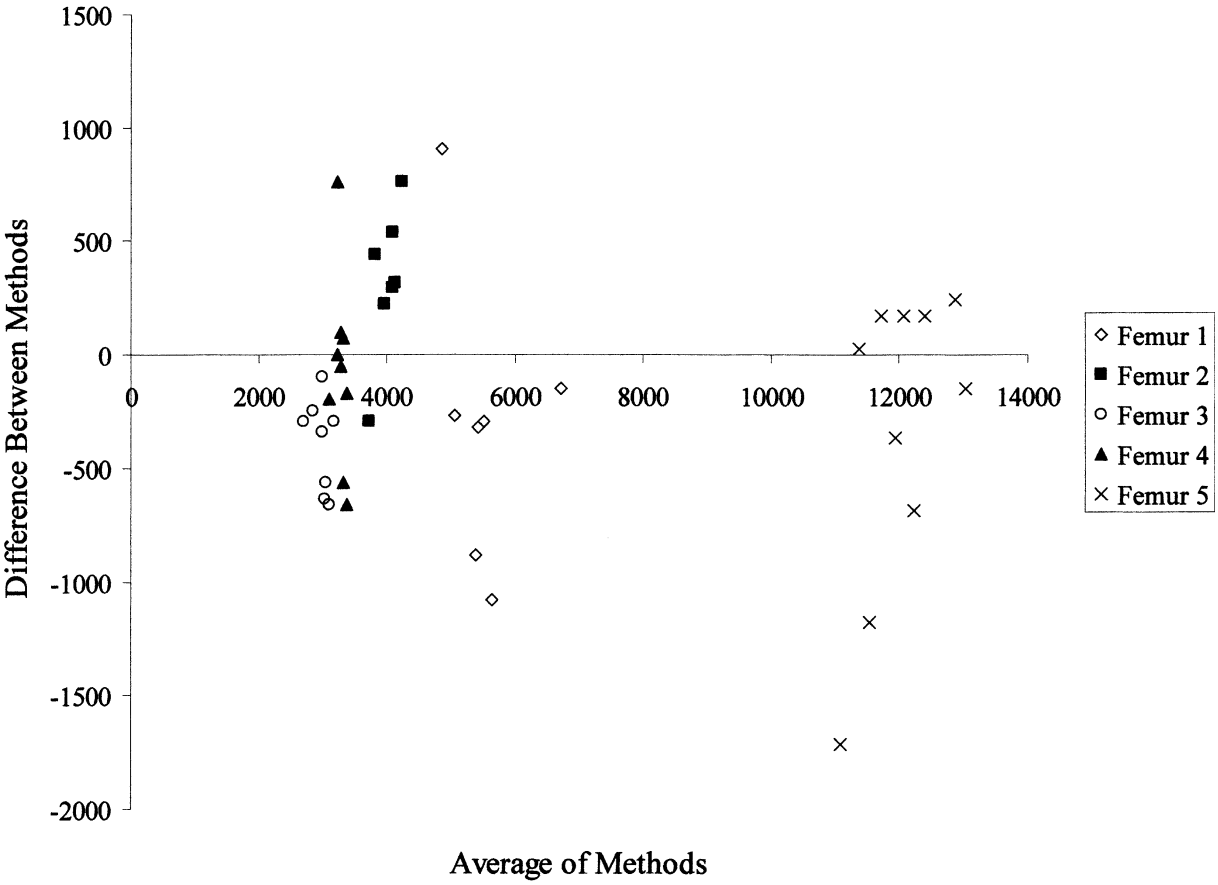


**Fig. 7.** Bland-Altman plot of the differences between methods for mean pore area (pors/mm$^2$).

spatial resolution of the scan, they are increasingly affected by this averaging effect [32]. Viewed from the inverse perspective, as scan resolution decreases, the partial volume effect takes an increasingly larger toll on the quality of the image and quantitative measures acquired from it, a relationship known as resolution dependency [33]. The partial volume effect coupled with median filtration, averaging of adjacent slices and segmentation, all contributed to the loss of smaller pores in the μCT slices. Although the results were promising at 10 μm, a higher scan resolution likely would have produced images that were more comparable to the microradiographs. The pore density values, in particular, would be improved due to the sharper delineation of smaller pores. This finding seems inconsistent with results of the study by Wachter et al. [17], which used a scan resolution of 30 μm and found that cortical porosity was accurately predicted by the μCT slices ($r^2$ = .90, linear regression). However, it should be noted that their sample population of older, total-hip-replacement patients was predisposed to elevated cortical porosity, which likely contributed to the level of predictability they obtained. Therefore, lower scan resolutions may prove useful in situations involving elevated porosity. Conversely, higher resolutions may be necessary for analyzing cortical porosity in small, non-human species, some of which have considerably smaller Haversian canals than do humans [34]. Ultimately, the tolerances of each experiment will dictate the necessary scan resolution and region of interest required to obtain meaningful results.

Although μCT can produce results comparable to conventional techniques for parameters related to cortical porosity, this technology has several limitations. Notably, μCT does not provide information related to bone dynamics, it can not differentiate between resorbing and forming surfaces, and it can not provide information regarding the orientation of collagen fibers [28, 29]. Engelke et al. [35] compared microradiographic and μCT image data and found that at 50-μm resolution, osteons were not discernable in μCT slices. The 10-μm resolution we employed likewise did not allow the visualization of density differences between osteons, lamellae, or cementing lines. As a consequence, no differentiation between pore types was possible in the μCT slices other than by pore shape (i.e., Volkmann canals) and size (i.e., resorption spaces). Scans at 5-μm resolution show some diffuse differences in mineral density between osteons [20], indicating that further improvement in scan resolution may overcome some of

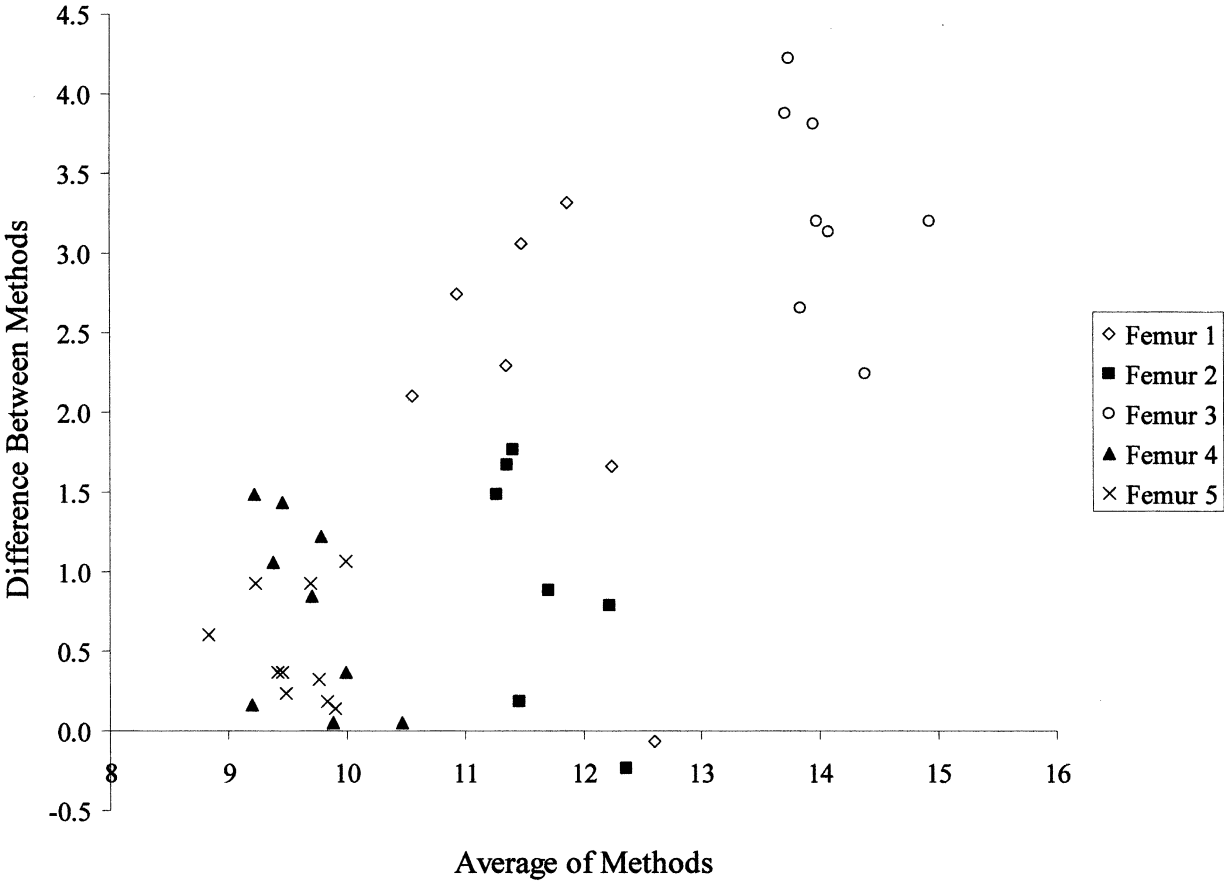


**Fig. 8.** Bland-Altman plot of the differences between methods for mean pore density ($\mu m^2$).

**Table 2.** Fully factorial nested analysis of variance (ANOVA) for comparison of the two methods

| Factor | *df* | MS | F | *P* |
|---|---|---|---|---|
| Cortical porosity | | | | |
| Method | 1 | 0.000515 | 48.843878 | < 0.001 |
| Sample | 4 | 0.02338 | 2215.2696 | < 0.001 |
| Method * Sample | 4 | 0.000038 | 3.619737 | 0.014 |
| Slices/Sections Nested within samples | 36 | 0.000053 | 5.015712 | < 0.001 |
| Error | 36 | 0.000011 | | |
| Mean Pore Area | | | | |
| Method | 1 | 481327 | 3.971239 | 0.054 |
| Sample | 4 | 265408000 | 2189.7758 | < 0.001 |
| Method * Sample | 4 | 319966 | 2.639913 | 0.050 |
| Slices/Sections Nested within samples | 36 | 336731 | 2.77823 | 0.001 |
| Error | 36 | 121203 | | |
| Pore density | | | | |
| Method | 1 | 46.950049 | 187.26845 | < 0.001 |
| Sample | 4 | 58.278954 | 232.45576 | < 0.001 |
| Method * Sample | 4 | 5.717996 | 22.807223 | < 0.001 |
| Slices/Sections Nested within samples | 36 | 0.435888 | 1.738613 | 0.051 |
| Error | 36 | 0.25071 | | |

these shortcomings. However, in our view, μCT imaging is best considered as a complement rather than as a replacement for existing methods, with the important advantage that μCT preserves samples for further correlative analysis (e.g., Wachter et al. [36]).

This study documents both the limitations and the promise of using μCT for measuring cortical bone porosity in two dimensions. The principal limitation was that significant, or nearly significant, differences were found between the μCT and microradiographic meas-

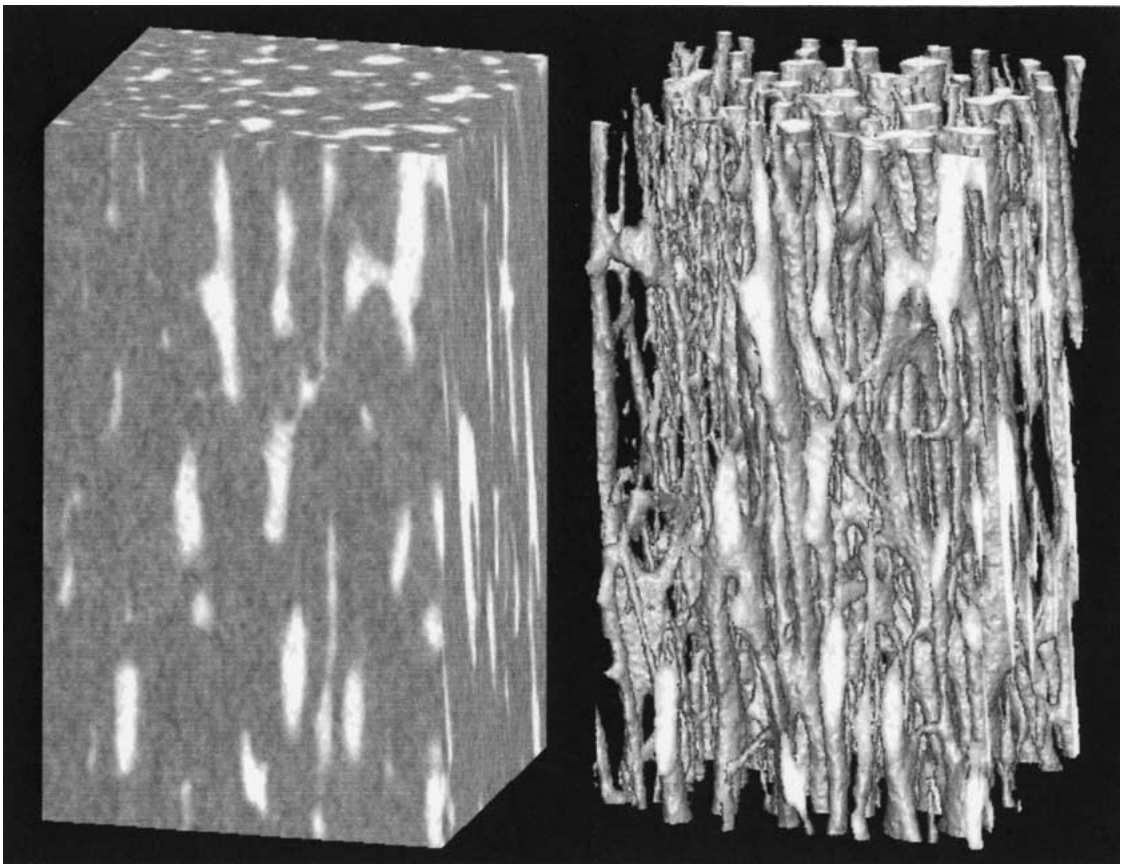

**Fig. 9.** Volumetric 3D reconstruction of 500 serial μCT images from Femur 5 (created with Analyze 4.0, Analyze Direct). Unsegmented volume on the left; thresholded volume demonstrating the pore network on the right.

urements. However, the biases between the techniques were relatively small, and repeatability for two of the three parameters was equivalent. We are very confident, therefore, that this technique is promising for the assessment of changes in cortical bone porosity associated with disease states and pharmaceutical intervention. For example, increases in cortical porosity due to primary hyperparathyroidism can be 3 times greater than those associated with osteoporosis [37], and should be easily detected by using 2D μCT. Conversely, the reduction of cortical porosity with bisphosphonate treatment over a 2 to 3 year period is on the order of 3.5% [38], a difference that would be detectable with 2D μCT.

Although we chose to produce composite 2D μCT slices for maximum comparability with the microradiographs, the μCT scanner was capable of generating much larger data sets. For example, within this study, the scans generated 90 contiguous (10-μm-thick) slices, potentially capable of producing 9 composite slices (100-μm-thick), from the same sample volume that produced a single ground section. Although 3D measures of cortical porosity were not obtained for the current study, 3D reconstruction of the serial slices provided an additional qualitative confirmation of the technique's potential (Fig. 9). Examining cortical porosity in three dimensions, as a network of canals, is a promising new application for μCT technology [20]. Achieving a better understanding of the 3D arrangement of cortical canals will provide new insights into the material properties and physiology of normal and pathologically altered cortical bone.

Many studies have described μCT as a fast and efficient method for the morphological analysis of trabecular bone, which provides a less destructive alternative to conventional histomorphometry. The aim of this study was to establish 2D μCT as a useful tool for the analysis of cortical bone, and thereby extend similar advantages to the study of cortical porosity. The qualitative and quantitative similarities we found between μCT slices and microradiographic sections affirms the use of 2D μCT for analysis of cortical porosity, and are particularly encouraging for the future exploration of higher scan resolutions.

*Acknowledgments*. We thank the anonymous reviewers for their constructive comments. This work was supported by the Canadian Foundation for Innovation (grant 3923), NSERC (Natural Science and Engineering Research Council of Canada, grant 238992-02), and Alberta Innovation and Science (grant URSI 01-103-R1) to B.H. J.R.M. receives operating support from the Canadian Institutes of Health Research, the

NSERC and the Canadian Arthritis Network. We thank the faculty and students of the Joint Injury and Arthritis Research Group for their assistance and insightful comments.

## References


1. Marotti G, Zallone AZ (1980) Changes in the vascular network during the formation of Haversian systems. Acta Anat (Basel) 106:84–100
2. Cohen JWH (1958) The three-dimensional anatomy of haversian systems. J Bone Joint Surg Am 40:419–434
3. Stout SD, Brunsden BS, Hildebolt CF, Commean PK, Smith KE, et al. (1999) Computer-assisted 3D reconstruction of serial sections of cortical bone to determine the 3D structure of osteons. Calcif Tissue Int 65:280–284
4. Hert J, Fiala P, Petrtyl M (1994) Osteon orientation of the diaphysis of the long bones in man. Bone 15:269–277
5. Petrtyl M, Hert J, Fiala P (1996) Spatial organization of the haversian bone in man. J Biomech 29:161–169
6. Currey JD (1988) The effect of porosity and mineral content on the Young's modulus of elasticity of compact bone. J Biomech 21:131–139
7. Martin RB, Ishida J (1989) The relative effects of collagen fiber orientation, porosity, density, and mineralization on bone strength. J Biomech 22:419–426
8. McCalden RW, McGeough JA, Barker MB, Court-Brown CM (1993) Age-related changes in the tensile properties of cortical bone. The relative importance of changes in porosity, mineralization, and microstructure. J Bone Joint Surg Am 75:1193–1205
9. Schaffler MB, Burr DB (1988) Stiffness of compact bone: effects of porosity and density. J Biomech 21:13–16
10. Barth RW, Williams JL, Kaplan FS (1992) Osteon morphometry in females with femoral neck fractures. Clin Orthop pp 178–186
11. Bell KL, Loveridge N, Reeve J, Thomas CD, Feik SA, et al. (2001) Super-osteons (remodeling clusters) in the cortex of the femoral shaft: influence of age and gender. Anat Rec 264:378–386
12. Jordan GR, Loveridge N, Bell KL, Power J, Rushton N, et al. (2000) Spatial clustering of remodeling osteons in the femoral neck cortex: a cause of weakness in hip fracture? Bone 26:305–313
13. Yeni YN, Norman TL (2000) Fracture toughness of human femoral neck: effect of microstructure, composition, and age. Bone 26:499–504
14. Yeni YN, Brown CU, Wang Z, Norman TL (1997) The influence of bone morphology on fracture toughness of the human femur and tibia. Bone 21:453–459
15. Tappen NC (1977) Three-dimensional studies of resorption spaces and developing osteons. Am J Anat 149:301–332
16. Jaworski ZF, Meunier P, Frost HM (1972) Observations on two types of resorption cavities in human lamellar cortical bone. Clin Orthop 83:279–285
17. Wachter NJ, Augat P, Krischak GD, Mentzel M, Kinzl L, et al. (2001) Prediction of cortical bone porosity in vitro by microcomputed tomography. Calcif Tissue Int 68:38–42
18. Bonse U, Busch F, Gunnewig O, Beckmann F, Pahl R, et al. (1994) 3D computed X-ray tomography of human cancellous bone at 8 microns spatial and 10(-4) energy resolution. Bone Miner 25:25–38
19. Cooper DML, Hallgrimsson B (2001) The application of 3D μCT to the analysis of cortical bone porosity. Am J Phys Anthropol 117:56.
20. Cooper DML, Turinsky AL, Sensen CW, Hallgrimsson B (2003) Quantitative 3D analysis of the canal network in cortical bone by micro-computed tomography. Anat Rec (in press)
21. Barbier A, Martel C, de Vernejoul MC, Tirode F, Nys M, et al. (1999) The visualization and evaluation of bone architecture in the rat using three-dimensional X-ray microcomputed tomography. J Bone Miner Metab 17:37–44
22. Barou O, Valentin D, Vico L, Tirode C, Barbier A, et al. (2002) High-resolution three-dimensional micro-computed tomography detects bone loss and changes in trabecular architecture early: comparison with DEXA and bone histomorphometry in a rat model of disuse osteoporosis. Invest Radiol 37:40–46
23. Ding M, Odgaard A, Hvid I (1999) Accuracy of cancellous bone volume fraction measured by micro-CT scanning. J Biomech 32:323–326
24. Fajardo RJ, Ryan TM, Kappelman J (2002) Assessing the accuracy of high-resolution X-ray computed tomography of primate trabecular bone by comparisons with histological sections. Am J Phys Anthropol 118:1–10
25. Ito M, Nakamura T, Matsumoto T, Tsurusaki K, Hayashi K (1998) Analysis of trabecular microarchitecture of human iliac bone using microcomputed tomography in patients with hip arthrosis with or without vertebral fracture. Bone 23:163–169
26. Kuhn JL, Goldstein SA, Feldkamp LA, Goulet RW, Jesion G (1990) Evaluation of a microcomputed tomography system to study trabecular bone structure. J Orthop Res 8:833–842
27. Muller R, Hahn M, Vogel M, Delling G, Ruegsegger P (1996) Morphometric analysis of noninvasively assessed bone biopsies: comparison of high-resolution computed tomography and histologic sections. Bone 18:215–220
28. Muller R, Van Campenhout H, Van Damme B, Van Der Perre G, Dequeker J, et al. (1998) Morphometric analysis of human bone biopsies: a quantitative structural comparison of histological sections and micro-computed tomography. Bone 23:59–66
29. Uchiyama T, Tanizawa T, Muramatsu H, Endo N, Takahashi HE, et al. (1997) A morphometric comparison of trabecular structure of human ilium between microcomputed tomography and conventional histomorphometry. Calcif Tissue Int 61:493–498
30. Altman DG, Bland JM (1983) Measurement in medicine: the analysis of method comparison studies. Statistician 32:307–317
31. Feldkamp LA, Goldstein SA, Parfitt AM, Jesion G, Kleerekoper M (1989) The direct examination of three-dimensional bone architecture in vitro by computed tomography. J Bone Miner Res 4:3–11
32. Kothari M, Keaveny TM, Lin JC, Newitt DC, Genant HK, et al. (1998) Impact of spatial resolution on the prediction of trabecular architecture parameters. Bone 22:437–443
33. Muller R, Koller B, Hildebrand T, Laib A, Gianolini S, et al. (1996) Resolution dependency of microstructural properties of cancellous bone based on three-dimensional μ tomography. Technol Health Care 4:113–119
34. Jowsey J (1966) Studies of Haversian systems in man and some animals. J Anat 100:857–864
35. Engelke K, Graeff W, Meiss L, Hahn M, Delling G (1993) High spatial resolution imaging of bone mineral using computed microtomography. Comparison with microradiography and undecalcified histologic sections. Invest Radiol 28:341–349
36. Wachter NJ, Augat P, Krischak GD, Sarkar MR, Mentzel M, et al. (2001) Prediction of strength of cortical bone in vitro by microcomputed tomography. Clin Biomech (Bristol, Avon) 16:252–256
37. Uchiyama T, Tanizawa T, Ito A, Endo N, Takahashi HE (1999) Microstructure of the trabecula and cortex of iliac bone in primary hyperparathyroidism patients determined using histomorphometry and node-strut analysis. J Bone Miner Metab 17:283–288
38. Roschger P, Rinnerthaler S, Yates J, Rodan GA, Fratzl P, et al. (2001) Alendronate increases degree and uniformity of mineralization in cancellous bone and decreases the porosity in cortical bone of osteoporotic women. Bone 29:185–191